

Dark Matter and Dark Forces from a supersymmetric hidden sector

S. Andreas*, M. D. Goodsell†, A. Ringwald‡

Deutsches Elektronen-Synchrotron, DESY, Notkestraße 85, 22607 Hamburg, Germany

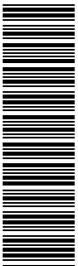
Abstract

We show that supersymmetric “Dark Force” models with gravity mediation are viable. To this end, we analyse a simple string-inspired supersymmetric hidden sector model that interacts with the visible sector via kinetic mixing of a light Abelian gauge boson with the hypercharge. We include all induced interactions with the visible sector such as neutralino mass mixing and the Higgs portal term. We perform a detailed parameter space scan comparing the produced dark matter relic abundance and direct detection cross sections to current experiments.

*sarah.andreas@desy.de

†mark.goodsell@desy.de, mark.goodsell@cern.ch

‡andreas.ringwald@desy.de



1 Introduction

There has been much interest recently in the possibility that there exists a hidden sector containing a dark matter particle coupled to a hidden $U(1)$ gauge boson (a “Dark Force”) having a mass of the order of a GeV that kinetically mixes with the photon [1–5]. Such a scenario could explain many astrophysical puzzles, such as the positron excess observed by PAMELA [6], ATIC [7], and Fermi [8], or the direct detection and annual modulation signals of DAMA [9], CoGeNT [10, 11] and CRESST [12] (if one ignores the disputed [13, 14] contradiction due to XENON100 [15] and CDMS [16]). Following from the work of [17–19], elegantly simple supersymmetric models in the latter category were constructed in [20] and further examined in [21] (see also [22]). However, these works emphasized that, in order to obtain such a light hidden sector, supersymmetry breaking effects in the visible sector would necessarily be dominated by gauge mediation, in order that the masses should be acceptably small. Thus it is natural to ask whether confirmation of these observations would be in contradiction with gravity mediation; in other words, whether it is also possible to have a gravity-mediated spectrum of particles that can yield similar phenomenology. This is also linked to the interesting question as to whether these models can be embedded into string theory: such hidden sectors appear very naturally there – see, e.g., [23–31] – but the problem of finding gauge mediation dominance over gravity mediation is notoriously difficult to achieve in globally consistent models.

Beyond the dark matter motivation, it is also useful to ask what hidden sector models of this form coming from string theory are allowed or excluded by current observations. This is because, even if the hidden sector does not comprise (all) the dark matter, there is a wealth of experiments capable of probing Dark Forces over a very wide range of hidden gauge boson mass and kinetic mixing values. Kinetic mixing was considered in the context of the heterotic string in [26, 32–35]. It has been examined in type II strings in [23–25, 36–40]; in [25, 29], both masses and mixings were considered, and it was argued that the Dark Forces scenario could be accommodated provided that there is additional sequestering. In this work, we shall consider hidden sector models with the particle content and similar couplings to those in [20], but argue that when we have gravity mediation domination, these can still give interesting phenomenological predictions under certain mild assumptions, without requiring additional sequestering relative to the visible sector. Although we will discuss the possible explanation of the signals found by DAMA and CoGeNT, these will therefore not be our primary motivation: rather, we wish to explore how simple supersymmetric hidden dark sectors with a hidden $U(1)$ can be constrained by observations.

The paper is organised as follows. In section 2, we describe the model of a supersymmetric dark sector that we shall be examining. This is followed by a summary of constraints upon hidden $U(1)$ s with hidden matter charged under them in section 3. There we also include the reach of future fixed target experiments and illustrate these with an investigation of a simple toy model. Section 4 then contains the meat of the paper: the results of the parameter search over our supersymmetric dark sector model. We include additional technical details in the appendix: the hidden sector renormalisation group equations (RGEs) in appendix A; the spectrum of the model in appendix B (including the mass mixing matrix with the visible neutralino in B.2); a review of kinetic and mass mixing of a massive hidden gauge boson with the hypercharge and Z in appendix C; and a description of the Goldstone boson mixing in appendix D. In addition, in appendix E, we discuss the supersymmetry-induced Higgs portal term and the mixing of the hidden and minimal supersymmetric standard model (MSSM) Higgs fields; we believe that although the existence of

the term has been known in the literature (see, e.g., [41] in non-SUSY models and [42] in the SUSY context) the effect of the mixing terms for direct detection have not been given elsewhere. Included is a calculation of the induced coupling of the hidden dark matter Majorana fermion to nucleons.

2 Supersymmetric dark sectors

2.1 Supersymmetric kinetic mixing

We shall consider models that interact with the visible sector primarily through kinetic mixing of a hidden U(1) gauge field with the hypercharge. Hence, we have a holomorphic kinetic mixing χ_h between hypercharge B_α with coupling g_Y (and gaugino the Bino, b) and hidden gauge superfield X_α with coupling g_h (and gaugino written as λ) appearing in the Lagrangian density

$$\mathcal{L} \supset \int d^2\theta \left(\frac{1}{4g_Y^2} B^\alpha B_\alpha + \frac{1}{4g_h^2} X^\alpha X_\alpha - \frac{\chi_h}{2} B^\alpha X_\alpha \right). \quad (2.1)$$

The physical kinetic mixing in the canonical basis [25, 39] is then given by

$$\chi = g_Y g_h \text{Re}(\chi_h). \quad (2.2)$$

We shall assume no matter charged under both hidden and visible gauge groups, so this relationship is valid at all energy scales. Since we are considering string-inspired models with a “hidden” U(1), that is, without matter charged under both the visible and hidden gauge groups, we shall take the value of the holomorphic kinetic mixing parameter to be of the order of a loop factor [25]:

$$\chi_h \equiv \frac{\kappa}{16\pi^2}. \quad (2.3)$$

Here, κ is a number that must, in principle, be derived from the high-energy model; in a field theory model, it is generated by integrating out some heavy linking fields (charged under visible and hidden sectors) at one loop, whereas in string models, it can be understood as arising from Kaluza-Klein modes of closed strings. In all cases, it depends only logarithmically upon mass splittings of the spectrum, and we shall therefore either take it to be equal to one or to vary by at most an order of magnitude from unity [25, 28, 29]¹. We thus have

$$\chi = g_Y g_h \frac{\kappa}{16\pi^2}; \quad (2.4)$$

the most commonly taken value for χ is thus of the order of 10^{-3} , but smaller values correspond to decreasing the hidden gauge coupling which may be extremely small in the case of hyperweak groups [25, 29, 44]. Henceforth, we shall always use the physical mixing χ .

As befits a well-studied subject, there are a variety of notations. In addition to using χ , we

¹Our results only depend on the absolute value of the mixing parameter. Effects that are sensitive to the different signs have been studied in [43].

shall also adopt the notation used in [45]:²

$$\begin{aligned} \chi &\equiv -\sin \epsilon \equiv -s_\epsilon \\ \cos \epsilon &\equiv c_\epsilon \equiv \sqrt{1 - \chi^2}, \quad \tan \epsilon \equiv t_\epsilon = -\frac{\chi}{\sqrt{1 - \chi^2}}. \end{aligned} \quad (2.5)$$

However, a crucial novelty in this work is the application of relation (2.4) to parameter scans rather than allowing for independent χ and g_h , which we shall see in section 3.4 will lead to qualitatively different results for the cross sections.

2.2 Hidden matter fields

The model that we shall consider is the simplest possible without adding dimensionful supersymmetric quantities. There are three chiral superfields S, H_+, H_- with H_+ and H_- charged under the hidden U(1) with charges ± 1 . These appear in a superpotential with dimensionless coupling λ_S

$$W \supset \lambda_S S H_+ H_-. \quad (2.6)$$

This is inspired by D -brane models where the singlet is essentially the adjoint of the gauge group: the superpotential above arises due to the $N = 2$ -like structure, and there is no renormalisable singlet potential due to this; alternatively, there may be $N = 2$ supersymmetry of the couplings at some scale, although we shall not enforce this. Such hidden sectors from string theory were considered in, e.g., [27, 31], and the above model was studied with gauge mediation in [20] where it was termed a ‘‘hidden sector NMSSM,’’ although we have set the cubic singlet term in the superpotential to zero. There then exists a global U(1) symmetry under which S and H_- are charged; string theory will not respect this, and we consider that it shall either be broken at higher order in the superpotential or through non-perturbative effects – but we shall assure that it will play no role in the following.

Once we include soft supersymmetry-breaking terms, we have the approximate potential for the hidden sector,

$$\begin{aligned} V &= |\lambda_S|^2 (|S H_+|^2 + |S H_-|^2 + |H_+ H_-|^2) \\ &\quad + \frac{g_h^2}{2} (|H_+|^2 - |H_-|^2 - \xi)^2 \\ &\quad + m_+^2 |H_+|^2 + m_-^2 |H_-|^2 + m_S^2 |S|^2 \\ &\quad + (\lambda_S A_S S H_+ H_- + \frac{1}{2} M_\lambda \lambda \lambda + c.c.), \end{aligned} \quad (2.7)$$

where $\xi = -\frac{\chi}{g_h} \xi_Y = \chi (g_Y/g_h) g_Y \frac{v^2}{4} \cos 2\beta$. The approximation lies in the D -term potential; the full form is found in appendix E.

A crucial difference for the phenomenology of the model once we consider gravity mediation is, however, that the gravitino is not the lightest supersymmetric particle (LSP), and therefore the dark matter can consist of stable hidden sector particles. We can thus perform a full analysis of the model, including the visible sector and its couplings, using micrOMEGAs [51–55] to determine the relic abundance and direct detection cross sections.

²Note, however, that this differs from the expressions in [20], which defines $\chi = -\tilde{\epsilon} \equiv -t_{\tilde{\epsilon}}, s_{\tilde{\epsilon}} \equiv -\frac{\chi}{\sqrt{1-\chi^2}}, c_{\tilde{\epsilon}} \equiv \frac{1}{\sqrt{1-\chi^2}}$, although there they write ϵ instead of $\tilde{\epsilon}$ (we added the tilde to avoid confusion with the above). On the other hand, [43, 46–50] define $\delta \equiv -\chi$.

2.3 Symmetry breaking through running

Just as in the MSSM, the top Yukawa coupling can, through running from the grand unified theory (GUT) scale, induce electroweak symmetry breaking, so in the model we are considering, the Yukawa coupling λ_S can induce breaking of the hidden gauge symmetry. By choosing the soft masses and couplings at the MSSM GUT scale we can then find models at the low-energy scale with hidden gauge symmetry breaking. *A priori* the independent supersymmetric parameters are χ, g_h, λ_S and the soft masses m_{H_\pm}, m_S, A_S and M_λ (the hidden gaugino mass) which we can choose at the high-energy scale and run down.

Via (2.4), we are asserting a relation between χ and g_h . Thus, if we take $\kappa = 1$, we reduce the number of free parameters in the model by one. However, as described above, we shall in certain plots (figures 3,5 right,6 right,7,8 right,9,10 right and 11) allow an order of magnitude variation in κ ; hence, although this does not strictly reduce the number of parameters in the model, it does rather constrain them with important consequences. Finally, we shall make one further assumption about the parameters: we shall take $m_{H_+} = m_{H_-}$ at the high-energy scale. This is motivated by the fields H_\pm being a non-chiral pair (note that we are taking no explicit Fayet-Iliopoulos term for the hidden $U(1)$ which would introduce a mass splitting). Otherwise, we shall scan over the remaining parameters to find interesting models.

The two-loop RGEs for the model are given in appendix A. By taking $m_S > m_{H_\pm}$ at the high-energy scale, the RGEs naturally drive the soft masses for $m_{H_\pm}^2$ to be negative at low energies, triggering hidden symmetry breaking.³ The visible sector coupling via the kinetic mixing then determines which field (H_+ or H_-) condenses; without loss of generality, we take χ to be negative, and thus H_+ condenses. Defining $\Delta \equiv \sqrt{\lambda_S^2 \xi - m_+^2 \lambda_S^2 / g_h^2}$, we have the conditions for a stable minimum with $\langle H_+ \rangle = \Delta / \lambda_S$ and all other expectation values zero:

$$\begin{aligned} 0 &\leq \Delta^2 \\ 0 &\leq m_-^2 + m_+^2 + m_S^2 + 2\Delta^2 \\ 0 &\leq (m_-^2 + m_+^2 + \Delta^2)(m_S^2 + \Delta^2) - |A_S|^2 \Delta^2. \end{aligned} \quad (2.8)$$

This is reviewed in appendix B. The hidden gauge boson mass is then given by

$$m_{\gamma'} = (\sqrt{2}g_h/\lambda_S)\Delta. \quad (2.9)$$

We give two examples of the values obtained scanning over m_S and $\alpha_S \equiv \frac{\lambda_S^2}{4\pi}$ in figure 1.

2.4 Symmetry breaking induced by the visible sector

The mechanism for hidden gauge symmetry breaking promoted in work such as [20] is via the effective Fayet-Iliopoulos term induced in the hidden sector by the kinetic mixing with the visible Higgs D -term. In such a case, the mass-squareds m_+^2, m_-^2 may be positive provided they are small enough that $\Delta^2 > 0$.

One motivation for this work is that such a case is more difficult to justify in the case of gravity mediation, but it is not implausible, since it can be achieved, for example, through sequestering

³We ignore the effect on the running of the kinetic mixing, since such terms always enter suppressed by $\mathcal{O}(\chi^2)$ [20] with an additional loop factor – and are thus equivalent to *three*-loop order. Of course, it would be interesting to include all of these effects, where then the hidden sector running would then be (extremely weakly) dependent upon the visible sector parameters, and we leave this to future work.

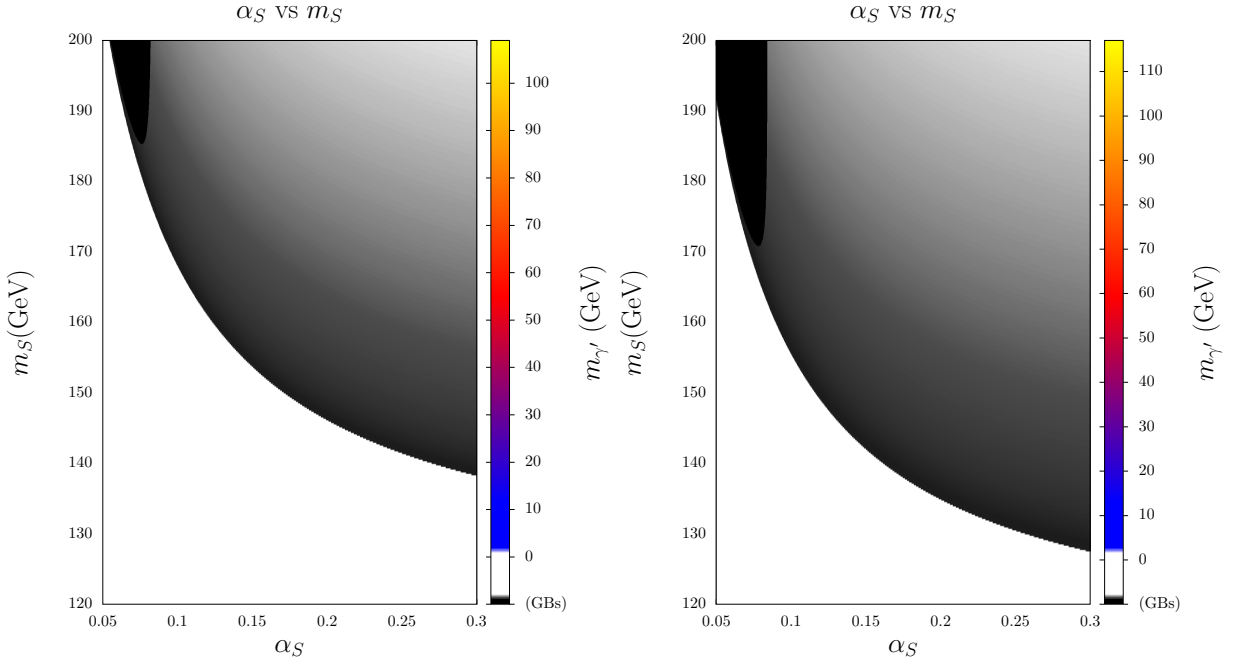


Figure 1: Hidden photon mass $m_{\gamma'}$ induced by radiative hidden gauge symmetry breaking, scanned over m_S and $\alpha_S \equiv \frac{\lambda_S^2}{4\pi}$. In both, $m_H = A_S = 100$ GeV, $\alpha_h = 0.0417$. *Left:* $M_\lambda = 71$ GeV, *right:* $M_\lambda = 50$ GeV. All values given at 10^{16} GeV. The black region shows no stable symmetry breaking.

of the hidden sector. In section 4, we shall examine this case, which is a qualitatively different scenario to that considered in [20], which considered gauge mediation. In the case of sequestering, we shall assume the gravitino to be much heavier than the hidden sector, but, importantly, that the singlet mass-squared $m_S^2 > 0$ and the hidden gaugino mass-squared M_λ^2 are of a similar order of magnitude to the hidden Higgs soft terms m_+^2, m_-^2 , while the hidden A_S term remains small. This is in contrast to gauge mediation where $m_S^2 \sim M_\lambda^2 \sim 0$.

2.5 Dark matter candidates

The model above contains essentially two different dark matter candidates: a Majorana fermion and a Dirac one.⁴ Neglecting the effect of kinetic mixing with the visible neutralino, the fermion mass matrix in the basis $(\tilde{\lambda}, \tilde{h}_+, \tilde{h}_-, \tilde{s})$ corresponding to hidden gaugino, hidden Higgsinos and hidden singlino is given by

$$\mathcal{M}_f = \begin{pmatrix} M_\lambda & m_{\gamma'} & 0 & 0 \\ m_{\gamma'} & 0 & 0 & 0 \\ 0 & 0 & 0 & \Delta \\ 0 & 0 & \Delta & 0 \end{pmatrix}. \quad (2.10)$$

⁴We are ignoring the possibility of scalar dark matter since, although the model as we have written it contains stable scalars, we expect the symmetries protecting them to be broken at some higher order in the potential allowing them to ultimately decay.

The Majorana particle is formed from diagonalising the $\tilde{\lambda}, \tilde{h}_+$ states; in the case of a large M_λ , this leads to a see-saw effect and a low mass. We shall refer to this state as “ \tilde{o}_1 ”, micrOMEGAs notation for the lightest odd particle. Clearly, there will therefore always be a fermion lighter than the hidden gauge boson (to avoid this fate, we would need to add a mass for the hidden singlino). In order for the Dirac fermion formed from \tilde{h}_-, \tilde{s} to be the lightest state, we would need $\lambda_S < \sqrt{2}g_h$ and for the Majorana mass M_λ to be rather small at the high-energy scale (this could happen, for example, in a string model where the modulus corresponding to the gauge coupling does not obtain an F -term), although it is somewhat suppressed in running down to the low scale. Hence, the Dirac fermion scenario is not compatible with radiative-breaking models, but presents an attractive candidate for the visible sector induced breaking. We shall refer to this state as “ \tilde{o}_7 ”. Note that this would not be a good candidate in gauge mediation, as there the singlet scalar would necessarily be lighter than the fermion [20].

In a complete analysis including the couplings and annihilation cross sections, it is necessary to take the mixing with the visible neutralino into account; this we do in appendix B.2.

Finally, we comment on the (lack of) effect of breaking the residual global symmetry on the above analysis. This could occur via terms in the super- or Kähler potential of the form S^n suppressed by an appropriate power of a mass scale, such as the string or Planck scale; for example, in string theory, it would be natural to expect terms of the form $S^n e^{-aT}$ where T is some modulus charged under a (broken) gauge symmetry from which the residual global symmetry descends – the effect could thus be *exponentially* suppressed by the expectation value of T , and so can, in principle, be naturally arbitrarily small. Since these are small effects, they will not affect the hidden gauge symmetry breaking (the singlet field would obtain a very small expectation value due to the radiative generation of a tadpole term in the potential, which would no longer be prohibited by the symmetry, but of course could be made arbitrarily small), but they will split the Dirac fermion into two Majorana ones with a potentially undetectable mass splitting. However, the lightest of these states, when it is the LSP, will be protected from decay by R-parity. This is important when considering the constraints of Big Bang Nucleosynthesis (BBN, and is in contrast to the cases considered in, e.g., [19]): in principle, any unstable relic with a lifetime greater than $\mathcal{O}(100)$ seconds must obey strict constraints on its density during BBN; see, e.g., [56]. On the other hand, the model does possess heavy scalars whose decays are protected by this symmetry, and also the heavier component of the Dirac fermion would then decay; however, since the effect can be arbitrarily small, we may simply assume that the lifetimes are many times that of the Universe, and so we can to all intents and purposes treat the symmetry as exact. This is our favoured perspective, but we can alternatively make the breaking strong enough that the scalars and heavier components can decay fast enough; for example, a coupling of the form $W \supset \lambda S^3$ will induce decays of S with $\Gamma \sim 10^{-2}\lambda^2 m_S$, so $\lambda \gtrsim 10^{-11}$ would suffice; similarly, a mass splitting of the fermions of Δm_Δ^2 will allow decays with $\Gamma \sim 10^{-2}|g_h \chi|^2 m_\Delta \frac{\Delta m_\Delta^2}{m_\Delta^2}$ which, for the values of the couplings considered in this paper, will suffice if $\frac{\Delta m_\Delta^2}{m_\Delta^2} \gtrsim 10^{-11}$. We will comment more upon BBN constraints in section 3.2.

3 Constraints and discovery potential

There are already a wealth of constraints on the parameter space of models with dark forces and hidden matter that we must apply in our search over models. However, there are also future experiments which will have the potential to rule further regions out – or make a discovery. In

this section, we summarise these current and future constraints and illustrate them by application to a toy model.

3.1 Limits on the hidden photon

A summary of various constraints on hidden photons from cosmology (including BBN), astrophysics and laboratory searches for the whole mass and kinetic mixing ranges $10^{-9} \text{ GeV} \leq m_{\gamma'} \leq 10^3 \text{ GeV}$ and $10^{-15} \leq |\chi| \leq 1$ has been presented for example in [57] and references therein. For the mass range of interest in this work, the constraints from electroweak precision tests (EWPT) are used as have been presented in [45], where the strongest constraint is provided by the mass of the Z for most of the parameter space. In the following plots (figures 4,5,6,8 and 9) of χ vs $m_{\gamma'}$, this is shown as a long-dashed approximately horizontal blue line excluding roughly $\chi \gtrsim 3 \times 10^{-2}$. Another constraint comes from the muon anomalous magnetic moment [58] and is dominant for $m_{\gamma'} < 1 \text{ GeV}$: in the above-mentioned plots of χ vs $m_{\gamma'}$, this is a dashed-dotted brown line at low masses and $\chi > 10^{-2}$. There is also a model-dependent constraint from BaBar searches [45] that might be the most constraining in the region $0.2 \text{ GeV} \lesssim m_{\gamma'} \lesssim 10 \text{ GeV}$ but only applies if the γ' can not decay into hidden sector particles; in the above-mentioned plots of χ vs $m_{\gamma'}$, this is a dashed dark purple line at low masses below 10 GeV and $\chi \sim 2 \times 10^{-3}$. This constraint does apply for most of the supersymmetric models we are considering, where the mass of the γ' and hidden matter are similar – preventing a decay of γ' to the hidden sector. However, if the hidden photon can decay to hidden matter, then there is instead a much weaker constraint from the Z width; we require

$$\frac{\Gamma(Z \rightarrow \text{hidden})}{\Gamma(Z \rightarrow \nu\bar{\nu})} \lesssim 0.008 \quad (3.1)$$

which for a single hidden Dirac fermion of mass $M_X < M_Z$ and unit charge under the hidden U(1) corresponds to (see also [59])

$$8c_W^2 s_W^2 \left(\frac{s_\phi}{c_e}\right)^2 \left(\frac{g_h^2}{e^2}\right) \left(1 + 2\frac{M_X^2}{M_Z^2}\right) \sqrt{1 - 4\frac{M_X^2}{M_Z^2}} \lesssim 0.008 \quad (3.2)$$

where c_W, s_W are the usual cosine and sine of the weak mixing angle respectively; s_ϕ is defined in equation (C.7). For $M_X \ll M_Z$, this simplifies to $\chi g_h \lesssim 0.04$. Clearly, for a small number of hidden particles (and $g_h < 1$), this is a weaker constraint than the measurement of the Z mass.

For $m_{\gamma'}$ below 1 GeV , there are additional constraints which are shown as grey areas in figure 3. The past electron beam dump experiments E141 [60], E137 [61] and E774 [62] have been reanalyzed in [63] in terms of hidden photons and were found to place limits on small masses $\lesssim 2m_\mu$. In addition, another such limit has been obtained from an electron beam dump experiment at Orsay [64] in [65]. Recently, two electron fixed target experiments A1 at MAMI in Mainz [66] and APEX at JLab [67] started, which are both searching for hidden photons behind a thin target from bremsstrahlung off an electron beam and which were already able to set first new constraints. Another limit arises in [68] from the reanalysis of data from a proton beam dump taken at the U70 accelerator at IHEP Serpukhov. At the Frascati DAΦNE ϕ -factory, the KLOE-2 experiment [69] set further constraints using e^+e^- collisions. However, not only are there limits on the kinetic mixing for very light hidden photons, but excitingly there are also dedicated

experiments planned (and partly already running) that can further probe this parameter space with real discovery potential. There are two fixed target experiments (A1 [66] and MESA) in Mainz and three (APEX [67, 70], DarkLight [71] and HPS [72]) at JLab. The estimated sensitivities of those experiments are shown in figure 3 for the toy model.

3.2 Constraints from Big Bang Nucleosynthesis

If a model produces too many high-energy photons, they can dissociate nuclei (such as lithium) and ruin the predictions from nucleosynthesis. The thresholds for these processes are of the order of a few MeV, and so photons produced with energies above this are potentially dangerous. This is typically used to constrain long-lived decaying particles where a photon is among the decay products; due to the rapid interactions of the photons with the plasma, a “zeroth order” spectrum of energies is produced with a cutoff at $m_e^2/(22T)$ (where m_e is the electron mass), and so these reactions only activate for temperatures T below 0.01 MeV, corresponding to times of the order of 10^4 s. The strongest constraints are for particles with lifetimes of 10^8 s. In models with a hidden sector, it is then natural to wonder whether visible photons can be produced, for example, by decays of particles in the hidden sector or the occasional annihilation of the frozen-out dark matter particles.

For a *massless* hidden photon, hidden sector matter does acquire a small charge under the visible photon (they become “millicharges”), in which case the constraints upon their presence during BBN are summarised in [57]. However, since we are considering a massive hidden photon, the diagonalisation of the physical states is given in equation (C.2), from which it can be seen that hidden sector states do not couple to the visible photon (cf. also (C.3)). Moreover, once a hidden photon is produced, the physical state does not oscillate into visible photons⁵ (so the constraints will be very different from, for example, possible sterile neutrinos). It does, however, couple to visible sector matter and decays with a width of $\Gamma \simeq \frac{1}{3}Q^2\alpha\chi^2c_W^2m_{\gamma'}$ into each light species of charge Q , i.e. $\Gamma > 10^{-2}\chi^2\text{GeV}$, or a lifetime $\tau_{\gamma'} < \left(\frac{10^{-11}}{\chi}\right)^2 \left(\frac{\text{GeV}}{m_{\gamma'}}\right)$ s. In this work, we shall be considering $\chi > 10^{-5}$, for which the hidden photon will always decay immediately on any cosmological timescales – and so there will be no relic density of hidden photons present.

From the above, we can see that BBN constraints will not affect our dark matter models in much the same way that they do not restrict standard weakly interacting massive particles (WIMPs). However, to be completely strict, let us consider that the annihilation of our dark matter particle will have some non-zero but small branching ratio into visible-sector photons, which we denote r_γ . One could imagine that this would arise from the plasma-induced mixing described above, where $r_\gamma \sim \chi c_W \frac{m_P^2}{m_{\gamma'}^2}$, but given the parameter region we are considering, this will be dominated by loop effects instead. Since the hidden $U(1)$ is not anomalous, the first diagram

⁵Recall that equation (C.2) is valid in a vacuum, and during BBN there is a small effect due to the thermal mass for the photon m_P in the plasma. Since we must consider temperatures below 0.01 MeV, below the electron mass, this is given by $m_P^2 \simeq 4\pi\alpha\frac{n_e}{m_e} \simeq 4\pi\alpha\frac{n_\gamma}{m_e}\eta$, where n_e, n_γ are the densities of electrons and photons, respectively, and η is the baryon-to-photon ratio. For $T = 0.01$ MeV, $\eta = 10^{-9}$, this gives an upper bound on the mass of $m_P \lesssim 10^{-8}$ MeV. The effect of this additional tiny mass is a minuscule orthogonal rotation of the physical states, whereby the photon and hidden photon mix by an amount $\chi c_W \frac{m_P^2}{m_{\gamma'}^2}$. If there were a relic population of hidden photons, in principle, a tiny fraction of them could oscillate into visible photons, and we would need to consider their effect on BBN – but, further, for the range of hidden photon masses and kinetic mixing we are considering here, this is clearly completely negligible.

appears at two loops, yielding $r_\gamma < \frac{\alpha^2}{(4\pi)^2} < 10^{-6}$.

The rate of annihilations of our dark matter candidate ψ into photons *per unit volume* (assuming that it annihilates entirely through the hidden photon channel) is $\Gamma_\gamma/V = r_\gamma n_\psi^2 \langle \sigma v \rangle$, where n_ψ is the relic density. The strongest bounds for BBN arise for particles of lifetime 10^8 s and constrain [56]:

$$m_\psi \frac{n_\psi}{n_\gamma} < 5.0 \times 10^{-12} \text{ GeV}. \quad (3.3)$$

We can therefore take a rough constraint by requiring that our relic particles never produce more photons than such a decaying particle; i.e. $\Gamma_\gamma/V < \frac{n_\gamma}{m_\psi} \times 5.0 \times 10^{-12} \text{ GeV}/10^8$ s for temperatures lower than 0.01 MeV. This yields, roughly,

$$r_\gamma \lesssim 2 \times 10^{-3} \left(\frac{0.01 \text{ MeV}}{T_c} \right)^3 \left(\frac{T_f}{50 \text{ MeV}} \right) \quad (3.4)$$

where T_f is the freezeout temperature (typically $T_f \sim m_\psi/20$) and we compare the rates at temperature $T_c < 0.01$ MeV. This is an overly conservative bound (since the largest disruptive effect of a decaying particle occurs at temperatures much below 0.01 MeV) but even so is very weak and will not affect the rest of our analysis.

3.3 Limits from dark matter

There are further experimental constraints arising on the dark matter particle, its mass and its interactions. First of all, the dark matter particle should not have a relic abundance in excess of the one measured by WMAP [73],

$$\Omega_{\text{DM}} h^2 = 0.1123 \pm 0.0035. \quad (3.5)$$

This is a very strict limit and translates to a lower limit on the dark matter (DM) annihilation cross section. We compute the dark matter relic abundance using micrOMEGAs where we have implemented our model. However, while there is an upper limit on the relic abundance, there is no objection to having a dark matter candidate whose abundance is lower than the one measured. In this case, it would then only be a part of the total dark matter (we shall refer to this as subdominant DM), and the remaining dark matter density would consist of other particle(s) such as an axion or axion-like particle whose phenomenology is not the subject of this article – we shall simply assume in such cases that the direct detection cross sections and interactions with the hidden sector of the additional dark matter are both negligible. In all of our plots, we show parameter points that give an abundance in agreement with the WMAP value in dark green and ones where the DM is subdominant in light green.

Additional constraints apply to the dark matter particle and its scattering cross section on nuclei. It is necessary to distinguish spin-dependent (SD) and spin-independent (SI) scattering. Depending on whether the dark matter particle is a Majorana or Dirac fermion, it has either dominantly SD or SI interactions, respectively. The SI interaction is, moreover, dominated by γ' exchange, which couples almost exclusively to the proton, particularly at low hidden photon masses (where the mixing can be treated as being effectively between the photon and hidden photon – see appendix C). The SI interaction is therefore strongly isospin-dependent, and we must rescale limits on the cross sections accordingly (which usually assume equal couplings for

protons and neutrons). For the SD interactions, however, the isospin dependence is rather weak, being dominated by Z exchange. Current limits from direct dark matter detection experiments are strongest for SI scattering cross sections ($\sim 10^{-42}$ cm²), while SD cross sections both on protons and on neutrons only start to be excluded at the 10^{-38} cm² level.

On the SI side, for the low dark matter masses (~ 10 GeV) we are interested in, the most relevant constraints come from XENON and CDMS. However, due to the signal claims from DAMA and CoGeNT,⁶ there has been a large debate on the reliability of those constraints, especially at low dark matter masses close to the energy threshold of the experiments. There are also large astrophysical (halo model, dark matter velocity and local dark matter density) and nuclear physics uncertainties that should be taken into account. Even though XENON and CDMS claim to rule out most of the DAMA and CoGeNT preferred regions, the positive signals remain and there have been various studies of how to reconcile those different results.⁷ We adapt the analysis of [81] which made a systematic scan taking into account the various uncertainties. There it is found that depending on the halo model, some of the CoGeNT and sometimes even DAMA preferred region is consistent with the exclusions from XENON and CDMS. For the details of the different halo models, see [81]; we will mostly use their so-called Standard Model Halo (SMH) and in a few cases show the differences that arise when changing for example to a Navarro-Frenk-White (NFW) or an Einasto profile.

We strictly apply the XENON100 and CDMSSi constraints derived in [81] to the SI scattering cross sections and only show points that are not excluded by any of the two experiments. In the plots of σ_p^{SI} ⁸ vs m_{DM} in section 4 (see figures 7 and 11), the CDMS limit is shown as a dashed turquoise line, while XENON100 is a dashed-dotted blue line. For most halo models, CDMS is more constraining at lower masses than XENON100.

In the SD case, there are both for scattering on protons and on neutrons several direct detection experiments sensitive to the low dark matter masses we are interested in. Different papers also tried to explain the DAMA signal by spin-dependent scattering either exclusively from neutrons [82] or from protons [83]. The former case is, however, not applicable in our models, as the spin-dependent cross sections of the Majorana fermion are always of the same order of magnitude both for protons and neutrons. In the latter analysis, it was shown that for scattering on protons, the DAMA favoured region is ruled out by Super-Kamiokande due to neutrinos from DM annihilation in the Sun almost independently of the annihilation channel. Additionally, the cross sections required in both scenarios are more than one order of magnitude above the largest ones that can be obtained in our models. Therefore, if the explanation of the DAMA (and CoGeNT) signals is confirmed as arising from spin-dependent scattering, it would rule out the models considered in this paper. Hence, we do not study this in more detail and simply apply the various spin-dependent scattering direct detection constraints. Until June 2011, PICASSO for the lightest and COUPP for the slightly larger masses were the most constraining experiments for SD scattering on protons [84]. Very recently, a new direct detection experiment SIMPLE [85] has published a limit on the SD scattering cross section on protons which in the low mass range is one order of

⁶We have not explicitly included the CRESST signal in our search. One of their two signal regions is roughly compatible with both DAMA and CoGeNT signals, although this is still subject to astrophysical uncertainties.

⁷One interesting possibility is to allow isospin-dependent interactions with just the right behaviour to suppress the interaction cross section with xenon nuclei [74–80]. We simply note that, although in the case of hidden Dirac fermions the interaction is almost entirely with protons rather than neutrons, in our models this tuning is not possible.

⁸We always show scattering from protons in the plots, hence σ_p^{SI} , since the constraints are strongest for these, and because our Dirac candidate will couple more strongly to protons than neutrons.

magnitude stronger than previous experiments (for a critique of their limit, see [86] and the collaboration’s response [87]). There is also a quite strong limit from Super-K using neutrino fluxes produced by dark matter annihilation in the Sun which, however, only applies to dark matter masses above 20 GeV (only neutrino-induced upward through-going muons have been used in this analysis which leads to a quite high-energy threshold and therefore a sensitivity only to larger DM masses) [88].⁹ For SD scattering on neutrons there are limits from XENON10 [90], Zeplin [91] and CDMS [16, 92, 93], the strongest of which, set by XENON10 for the mass range of interest in this paper, is less constraining than the SIMPLE limit.

In the following analysis, we use all constraints from SD scattering both on protons and on neutrons with the exception of SIMPLE as strict exclusions and show only points consistent with those limits. As there has been criticism of SIMPLE’s limit, we will not apply this universally but rather show how our results change when taking it into account. In the plots of σ_p^{SD} vs m_{DM} in section 4 (see figures 7 and 10), the exclusion lines for the different experiments are as follows: SIMPLE short-dashed brown line, Super-K dashed black line, PICASSO long-dashed orange line, COUPP2011 dashed-dotted turquoise line, COUPP2007 dotted blue line and KIMS long-dashed green line. The plots of σ_n^{SD} vs m_{DM} in the same figures show the limits of XENON10 as dashed-dotted blue, Zeplin as dotted pink and CDMS as dashed turquoise lines.

Those constraints on the scattering cross section can strictly only be applied to particles that actually constitute the entire dark matter density. If the dark matter is subdominant however, the limits on its scattering cross section have to be rescaled accordingly: the local density ρ_ψ of a dark matter candidate ψ relates to the local total DM density ρ_{DM} as their abundances

$$\frac{\rho_\psi}{\rho_{\text{DM}}} = \frac{\Omega_\psi}{\Omega_{\text{DM}}} \quad (3.6)$$

and so do the limits that are set by direct detection (DD) experiments. Thus, an experimental bound on σ_{DD} translates into an actual bound on the scattering cross section σ_ψ of ψ as

$$\sigma_\psi = \sigma_{\text{DD}} \frac{\Omega_\psi}{\Omega_{\text{DM}}}. \quad (3.7)$$

This means that direct detection constraints on the scattering cross section become less potent for subdominant DM particles.¹⁰

3.4 Application to toy model

To illustrate the above constraints/future experimental reach, and more importantly provide a comparison to the more complete model of section 2 that we shall investigate in section 4, here we shall consider a toy model. This is the simplest possible dark sector: a Dirac fermion ψ with unit charge only under the (massive) hidden U(1). We shall not include any Higgs sector – the U(1) could, after all, naturally have a GeV scale mass via the Stückelberg mechanism [25, 29] – so we will not consider how the dark matter particle becomes massive. This is essentially the model considered in [46–50] except that we shall insist on the relation (2.4); the parameters are the dark matter mass m_ψ , hidden photon mass $m_{\gamma'}$, kinetic mixing χ and the tuning parameter κ .

⁹There is another more recent analysis [83] with limits for smaller masses. Application of these limits taking into account the annihilation details and branching ratios is beyond the scope of this work and left for future works [89].

¹⁰This is obviously based on the reasonable assumption that the local DM has the same content of different DM contributions as averaged over the whole Universe.